VNU Journal of Science: Mathematics - Physics

Journal homepage: https://js.vnu.edu.vn/MaP

Original Article

The Photothermal Effect of a Single Gold-magnetic Nanocrescent in A Glycerol-water Mixture Media

Pham Thi Thu Ha, Vu Xuan Hoa*, Tran Thu Trang

TNU-University of Sciences, Tan Thinh, Thai Nguyen, Vietnam

Received 04 January 2023
Revised 11 February 2023; Accepted 16 February 2023

Abstract: The photothermal effect of gold nanostructures has been majority known as the nanothermal effect of gold clusters under laser irradiation. However, there are still many challenges to measuring the local temperature generated by a single nano gold in a complex media. In this work, a gold magnetic nanocrescent (G-MNC) has been studied, it composed of a superparamagnetic iron oxide core and gold shell with a size of 170 nm in glycerol/water (80:20), under 650 nm laser irradiation. Using rotational scattering correlation spectroscopy (RSCS), a sophisticated technique has been developed, the local temperature generated by only single magnetic nanocrescent was measured. The dependence of the heat generation according to the power of the laser shows that the heat generated by the gold NC is proportional to the power of the laser, and the maximum temperature was 19.5 ^{o}C, corresponding to the laser power was 29×10^{3} W.cm^{-2}. Under using the proper laser irradiation to the plasmon resonance, G-MNCs act as nano thermometers. The photothermal effect of the single G-MNC was implemented in a mixing solution of glycerol and water.

Keywords: Gold-magnetic nanocrescent, Local temperature, Brownian motion, Surface plasmon resonance, Dark-filed microscope.

1. Introduction

Currently, many research groups have special interests in studying potential applications of photothermal effects in the biomedical field [1-6]. Novel metallic nanoparticles (gold nanoparticles, gold nanorods, gold multilayer nanoparticles, multilayer coating of gold nanoparticles, gold nanocrescents, etc.) are known to possess unique optical properties due to their surface plasmon resonant [7, 8]. Scattering and absorption intensities cross sections of gold nanoparticles are a few times larger

* Corresponding author.
E-mail address: hoavx@tnus.edu.vn

https//doi.org/10.25073/2588-1124/vnumap.4801

than those of fluorescent dyes classically used for biomedicine imaging [9]. The research on the photothermal effect of plasmonic nanostructures has also been engaging in many groups, such as [3], [9-11]. Particularly, the Fresnel Institute, a France research group, has studied the photothermal effect in both theorecical and experimental research. They used metallic nanoparticle structures as thermoplasmonic sources [12]. Here, it has been found that when the excitation light frequency is equal to the surface plasmon resonance frequency of the nanoparticle, the optical absorption efficiency is significantly increased. Besides, the local photothermal effects of a single gold nanoparticle in environments (water, complex environment, environment of biological imitation) were carefully studied by the group of Richardson and Quidant [12, 13]. By fabricating nanoparticles with different shapes and sizes, the strong plasmon absorption wavelengths in the spectral region corresponding to the weak absorption of biological environments will be revealed. In this window, one can heat the nanoparticles locally while their surrounding does not absorb the excitation light.

In 2005, Liu et al., [13] initiated the fabrication of gold nanocrescents (GNC) by a physical method for Surface Enhance Raman Scattering (SERS) application. Nanocrescents were synthesized by a nanosphere lithography technique. A thin layer of metal was deposited on dielectric nanoparticles spin-coated on a glass substrate. Thus, it is possible to extend the active region of the surface plasmon resonance scattering and absorption. Subsequently, there have been more researches on the optical properties of these asymmetric nanoparticles [15-19]. However, researches on the photothermal properties of these singles in the biology medium are still very limited.

Extending our previous works, which mainly focused on studying the photothermal effect of a single nano in glycerol [20], we report the photothermal effect of only a single GNC in a complex media involving glycerol (80%) and water (20%). Gold magnetic nanocrescents **(**G-MNC) were fabricated by the electron-beam deposition (EBD) technique. The optical system was designed and developed based on a dark-field microscope using a module crop-mode and an afocal system to modulate the signal into the detector and focus the laser beam on a sample. The morphological property of G-MNC was studied by the transmission electron microscope (TEM). The UV-vis absorption and scattering spectroscopies were used to examine the sample's optical properties. The local temperature of the single G-MNC was determined by Rotational scattering correlation spectroscopy (RSCS), which based on the Brownian rotational motion of anisotropy nanoparticles [20].

2. Materials and Methods

2.1. Synthesized Gold-magnetic Nanocrescent

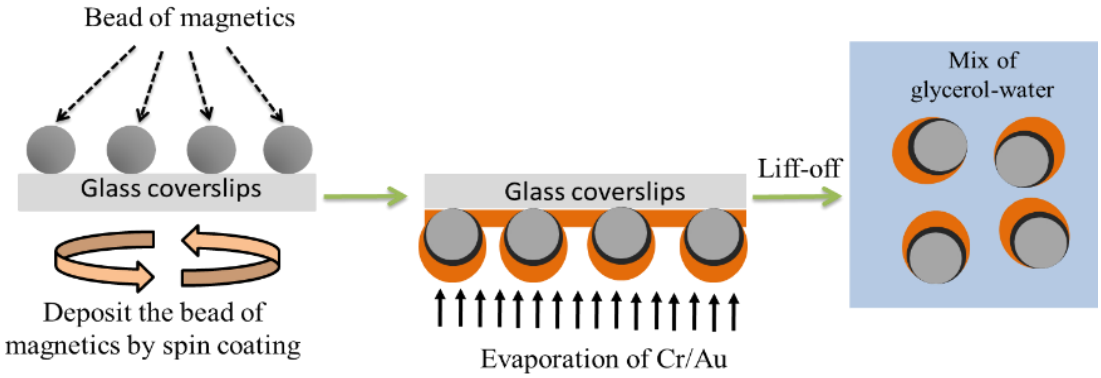

Figure 1. The schematic processes for G-MNCs fabrication by using the EBD method.

The methods to fabricate gold magnetic nanocrescents were reported [20, 21]. In this work, G-MNCs were synthesized by EBD method. The schematic diagram for fabrication is shown in Fig. 1. In the initial step, superparamagnetic nanoparticles (Fe_3O_4, ~ 140 nm in diameters) were spined coating on glass coverslips with the rotation of the substrate at speed (1,000 rpm) in ten minutes to gain a homologous contribution on the surface. Then, 30 nm gold nanostructures were evaporated to cover G-MNC after the evaporation process of 2 nm Cr to enhance the adherence between Au and superparamagnetic nanoparticles. Finally, G-MNCs were gently separated from the glass substrate by a brush and stored in a mixing solution of glycerol/water (80:20). A strong magnet was used to wash the residue gold magnetic particles colloid to obtain purer G-MNCs.

2.2. Optical Configuration Setup

The optical configuration was designed to monitor and gain the kinetic images of single G-MNCs in the complex environment, glycerol/water, as shown in Fig. 2. This configuration system was set up by our group and reported in the previous work [20]. Briefly, a dark-field microscope composed of an X20 objective lens (NA = 0,45) was used to collect the scattering signal from the sample and transfer it into the camera to obtain the image of G-MNC. To observe the dark-field images of a single G-NMC, a white light source was shined through a condenser (NA = 0.80 - 0.95) to reach the sample. One "Crop Mode" module configuration was added in this configuration to increase the acquisition time of the camera; thus, this setup can easily manipulate the RSCS method to measure rotation time (τ_r) of a single nanoparticle. A red laser at 650 nm was used to focus on the sample, which was dispersed in the mixing solution glycerol/water, to shed light on the photothermal effects of an individual nanoparticle. An external power supply can modulate the power density of the red laser. The mix of glycerol-water does not absorb light in the visible region (Fig. 5) [22]. There fore the sample is heated up due to the thermal dissipation of G-MNC. With our optical configuration setup, the power density of the red laser on the sample can reach $2.9x10^3$ W/cm^2. The insert figure in Fig. 2 is the dark-field image of G-MNCs collected by this setup.

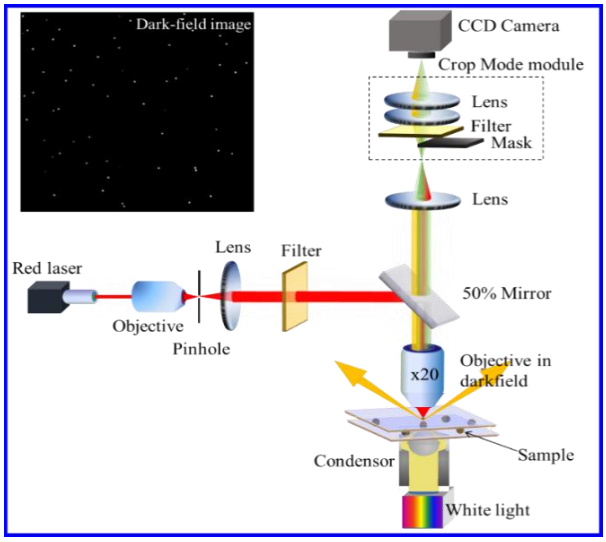

Figure 2. Designed Optical configuration to observe and heat an individual G-MNC by a red laser. The figure inset is the dark-field image of G-MNC.

3. Results and Discussion

3.1. Morphologies of Gold Magnetic Nanocrescent

TEM was carried out to characterize morphologies of G-MNC. Fig.3 presents the TEM images of two single G-MNC with crescent structures composed of a dark half is gold metal covering the superparamagnetic iron oxide with a diameter of about 140 nm. Fig. 3b, 3c and 3d show the scanning electron microscopy (SEM) and atomic force microscopy (AFM) images of G-MNC, respectively. Fig. 3c depicted the morphology 2D of the sample which shows that the maximum deeply of G-MNC is 170 nm. This value agrees with TEM image. The image inset in Fig. 3d is profile of G-MNC. Thus, these images clearly indicate the shape of G-MNC and again confirm the fabrication processes success.

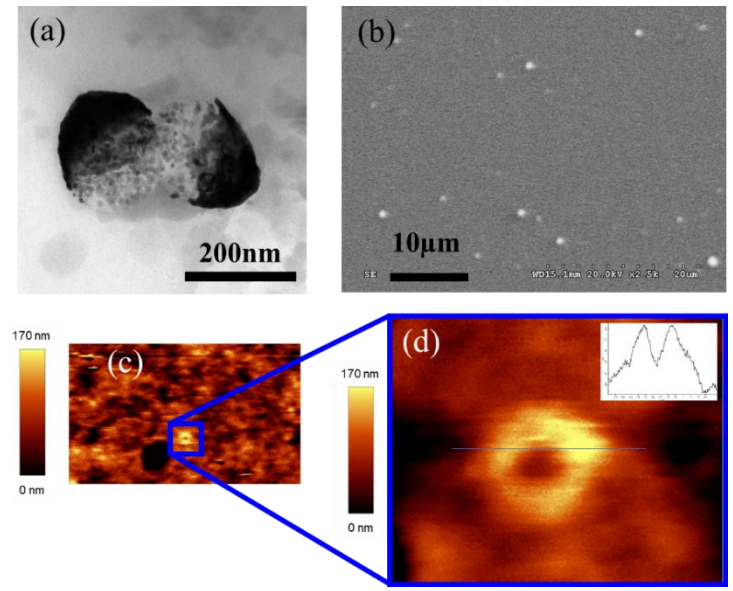

Figure 3. (a) TEM image of gold-magnetic nanocrescent (G-MNC). It is composed of the gold semi-shell, the polymeric nanosphere, and the magnetic nanocrystals embedded in the polymer; (b) SEM of G-MNC; (c, d) AFM image of a G-MNC at different magnifications.

3.2. Gold-magnetic Nanocrescent as a Thermal Source

Upon excitation at 640 nm, G-MNC in glycerol/water will absorb the photon's energy and generate heat; as a result, we can consider each G-MNC as a thermal source. However, to attain the generated temperature of only G-MNC, we have to measure its hydrodynamic radius (R_h). As previous works indicated [20], R_h can be achieved from mean square displacement (MSD) and perform a linear fitting to determine the diffusion coefficient in two dimensions. In this case, particulars move in an environment with viscosity coefficient - μ(T) at temperature T.

According to the Stokes-Einstein relation, the MSD can be calculated as:

$$\langle \Delta r^2(\Delta t) \rangle = 4D.\Delta t \tag{1}$$

where Δt is the elapsed time and D is the translational diffusion coefficient.

$$D = \frac{k_B T}{6\pi \mu_m(T) R_h} \tag{2}$$

where $R_h = \frac{1}{2}\left(\frac{6V_h}{\pi}\right)^{\frac{1}{3}}$ is the hydrodynamical radius, $\langle \Delta r^2(\Delta t)\rangle$ is measured at room temperature, using a free particle-tracking algorithm [23], k_B and $\mu_m(T)$ are the Boltzmann constant and viscosity of mix glycerol/water. $\mu_m(T)$ were determined by Cheng formula [24]:

$$\mu_m(T) = \mu_w^{\alpha}\mu_g^{1-\alpha} \quad (3)$$

In which $\alpha = 1 - C_g + a * b * C_g + (1 - C_g)/(a * C_g + b * (1 - C_g))$

$\mu_w = 1.790 * exp\left(\frac{(1230-T)T}{36100+360*T}\right)$ is the viscosity of water, $\mu_g = 12100 * exp\left(\frac{(1233+T)T}{9900+70*T}\right)$ is the viscosity of glycerol,

a, b are constants and were defined by: $a = 0.705 - 0.0017T$

$$b = (4.9 + 0.036T)a^{2.5}$$

C_g is the concentration of glycerol.

The translational diffusion coefficient D was easily deduced from fitting the experimental value of MSD with theory former (see Eq. (1)). At room temperature (23°C), $\mu_m(T)$ can be calculated by the formula of Cheng [24] (Eq. (3)). The value of the MSD of a typical G-MNC was calculated from Fig. 4b, then R_h was found 84 nm. This value is rather suitable with TEM and SEM images. Figure 4a shows typical Brownian trajectory of an individual G-MNC tracked with a free particle-tracking algorithm.

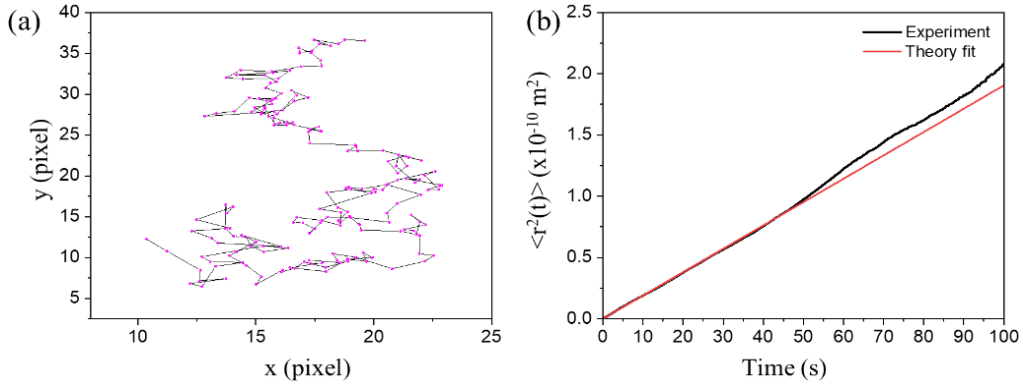

Figure 4. (a) Typical Brownian trajectory of an individual G-MNC in mix glycerol-water. (b) Mean square displacement (MSD) respectively.

Now, we will estimate the local temperature generated by a single G-MNC under laser irradiation at 650 nm in a mixing solution of glycerol/water (80:20). It should be noted that under laser excitation at 650 nm, the mixing solution does not absorb the photon of laser due to the range absorbance of glycerol is at the ultraviolet range, as depicted in Fig. 5. Whereas the plasmon bands of G-MNC are at 550 nm and 650 nm corresponding to the transerve and longitudinal plasmon bands, respectively. Thus, the longitudinal band is coincident with the laser excitation; consequently, the heat generated after irradiation comes from only G-MNC. It is known that a G-MNC in a solution attends both translation and rotation motions. Translation motion is due to the natural Brownian motion, and rotational motion is the result of asymmetry in the shape of a G-MNC [25]. The asymmetrical shape of NCs induces a splitting of the plasmon resonance, and that property allows one to follow the rotational dynamics of the orientation of gold nanocrescent [26, 27]. Therefore, the scattering signal of G-MNC flickers and varies in intensity (Figs. 6a, 6b) [28]. Due to this blinking of scattering signal, we have continuously developed a model of autocorrelation RSCS of the work to evaluate the local heat generated by a single G-NMC

in glycerol/water (80:20). Briefly, in the experiment, the RSCS is calculated using the autocorrelation function of the intensity $I(t)$ as:

$$G(\tau) = \langle I(t)I(t+\tau)\rangle \quad (4)$$

$G(\tau)$ depends on the rotational diffusion properties and the setup geometry. The autocorrelation function $G(\tau)$ can be calculated by:

$$G(\tau) = \frac{1}{4\pi}\sum_{l=0}^{\infty} c_l^2 e^{-l(l+1)\tau/2\tau_r} \quad (5)$$

where c_l is a factor in the calculation of spherical harmonics, and τ_r is the Brownian relaxation time given by Debye - Einstein – Stockes relation:

$$\tau_r = \frac{3\mu_m(T)V_h}{k_B T} \quad (6)$$

where k_B is the Boltzmann constant.

$G(\tau)$ is a multi-exponential function which can be defined in the experiment $\langle I(t)I(t+\tau)\rangle$. τ_r is the relaxation time as the only parameter. The local temperature can be easily obtained from τ_r by fitting the experimental autocorrelation intensity function with Eq (6).

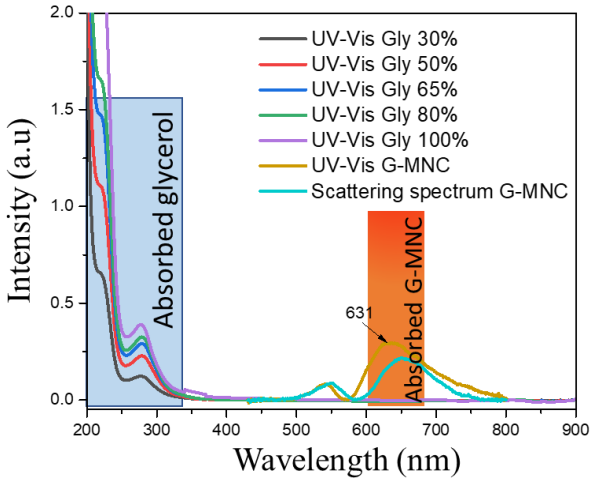

Figure 5. Absorption spectra of the glycerol and water mixing solution with glycerol concentration varying from 30% to 100%; and absorption and scattering spectra of G-MNC in the mixing solution glycerol/water (80:20).

Fig. 6c is a typical result obtained using the autocorrelation function $G(\tau)$ with the signal from Fig. 6b. The result indicates a well-fitting between practical data and fitting function.

We now focus on using RSCS to measure local temperature T under the excitation of red lasers for the same gold NC. A gold-magnetic nanocrescent is heated by a red laser in mixed glycerol/water. The power of the laser was adjusted at 480, 5800, 16000, and 29000 W/cm^2. Fig. 7a depicts the autocorrelation functions obtained for the different powers of the red laser. The correlation time decreases clearly as the laser power increases, indicating a local rise in temperature. The local temperature is deduced from the value of τ_r. The values τ which correlate to these above laser powers excitation is 18.3 ms, 12.12 ms, 9.4 ms, and 7.6 ms, respectively (Fig. 7b). These results are well appropriate with the theory (Eq. 6). The local temperature variation depends on the power of the incident laser, as described in Fig. 8. If neglecting the interaction between the laser and the magnetic core,

increasing the laser power led to an increase in the vicinity temperature of the G-MNC. Experimental result shows that the temperature distribution around nanoparticle is inhomogeneous, and the measuring local temperature was maximum on the surface of the particle ($r = R_h$). At the maximum laser power, the local temperature of G-MNC was 19.5 °C; this is higher than the value obtained in the experiment implemented in the pure glycerol [20]. It is proper due to the coefficient of viscosity of glycerol being higher than that of water; then the viscosity of mixing solution glycerol/water is smaller than that of pure glycerol, leading to the faster rotation motion, decrease of τ_r, and increase of temperature [29].

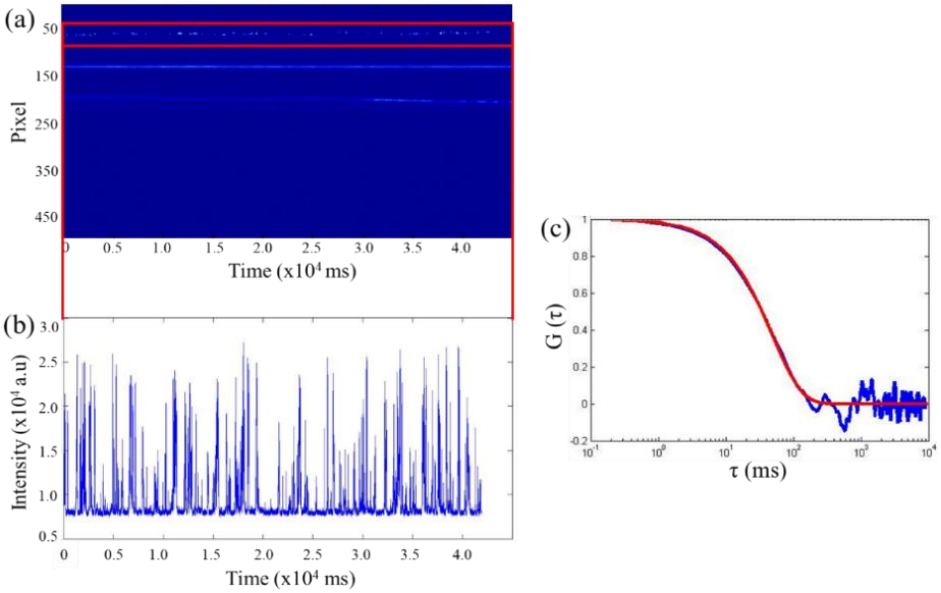

Figure 6. (a) The cartography of the scattering signal and (b) its scattering signal intensity of a typical G-MNC; (c) RSCS image extrapolated from scattering signal intensity of (b).

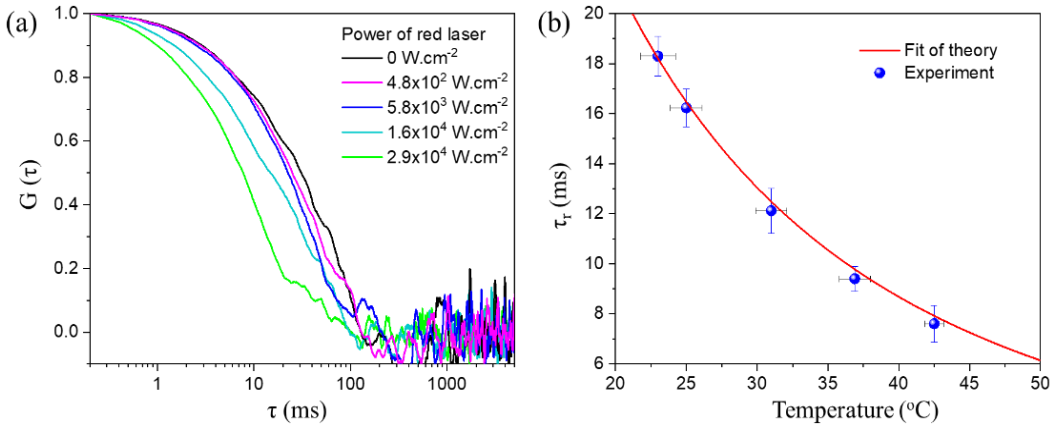

Figure 7. (a) Autocorrelation functions of RSCS of only single G-MNC under varying the power of the laser; (b) Recovery Brownian time and respective local temperature were extrapolated from (a).

Figure 8 shows the local temperatures in the vicinity of the G-MNC deduced from the values of τ_r as a linear function of the power of the incident red laser via $P = 6.2\text{x}10^{-4}T + 24.52$ with $R^2 = 0.989$. The temperature increases by 19.5 °C compared to the ambient temperature at the maximum power of red

laser irradiation. It can be easily realized that the efficency of photothermal effects depends on the laser wavelength irradiation. When the laser excitation overlaps with the surface plasmon resonance band, the efficiency of photothermal effect is optimized. In this work, upon laser excitation at 650 nm, the local temperature of a G-MNC, which corresponded to the highest power laser excitation, achieved the best efficiency of the photothermal effect (Fig. 5).

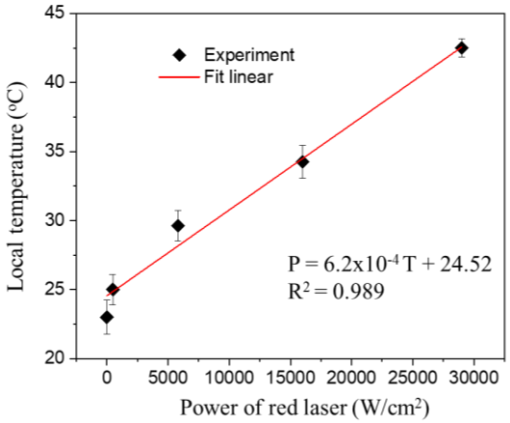

Figure 8. The local temperature of only a single G-MNC depends on the power of laser excitation at 650 nm.

4. Conclusion

In this work, we took advantage of a familiar method which normal uses to fabricate thin metal film to synthesize asymmetric G-MNCs nanocomposites. Thanks to the optical asymmetry of G-MNC and using RSCS, the local temperature of only a single G-MNC in mixing solution glycerol/water (80:20) was estimated under laser irradiation at 650 nm. The photothermal effect efficiency was optimized because the laser excitation wavelength almost coincided with the plasmon band of G-MNC. This result shows a good fitting between experimental data and theoretical one. Moreover, by using laser excitation, each G-MNC can act as a thermal source, making them a promising material for application in nanotechnologies, such as control and measurement of local temperature from a far distance, especially in complex environments like membranes.

Acknowledgements

This research is funded by Vietnam National Foundation for Science and Technology Development (NAFOSTED) under grant number 103.03-2020.43.

References

[1] H. N. Tran et al., Optical Nanoparticles: Synthesis and Biomedical Application, Adv. Nat. Sci. Nanosci. Nanotechnol., Vol. 6, No. 2, 2015, pp. 23002, https://doi.org/10.1088/2043-6262/6/2/023002.

[2] P. Tuersun, X. Han, Optical Absorption Analysis and Optimization of Gold Nanoshells, Appl. Opt., Vol. 52, No. 6, 2013, pp. 1325-1329, https://doi.org/10.1364/AO.52.001325.

[3] G. Palermo, D. Pagnotto, L. Ricciardi, L. Pezzi, M. L. Deda, A. D. Luca, Thermoplasmonic Effects in Gain-Assisted Nanoparticle Solutions, J. Phys. Chem. C, Vol. 121, No. 43, 2017, pp. 24185-24191, https://doi.org/10.1021/acs.jpcc.7b08186.

[4] R. Khursheed et al., Biomedical Applications of Metallic Nanoparticles in Cancer: Current Status and Future Perspectives, Biomedicine & Pharmacotherapy, Vol. 150, No. 112951, 2022, pp. 1-24, https://doi.org/10.1016/j.biopha.2022.112951.

[5] S. Jeong, J. Young Park, J. Min Kim, Y. Kim, Photothermally Enhanced Hollow Gold Nanopigment for Water Evaporation and Sterilization Achieved Via A Photothermal Effect, Buil. And Envi., Vol. 229, No. 109970, 2023, pp. 1-8, https://doi.org/10.1016/j.buildenv.2022.109970.

[6] Y. Shen, Y. Zou, B. Bie, C. Dong, Y. Lv, Combining Dual-Targeted Liquid Metal Nanoparticles with Autophagy Activation and Mild Photothermal Therapy to Treat Metastatic Breast Cancer and Inhibit Bone Destruction, A. Bio., Vol. 157, 2023, pp. 578-592, https://doi.org/10.1016/j.actbio.2022.11.044.

[7] M. Sriram, K. Zong, S. R. C. Vivekchand, J. J. Gooding, Single Nanoparticle Plasmonic Sensors, Sensors (Switzerland), Vol. 15, No. 10, 2015, pp. 25774-25792, https://doi.org/10.3390/s151025774.

[8] X. Huang, M. A. E. Sayed, Plasmonic Photo-thermal Therapy (PPTT), Alexandria J. Med., Vol. 47, No. 1, 2011, pp. 1-9, https://doi.org/10.1016/j.ajme.2011.01.001.

[9] R. S. Riley, E. S. Day, Gold Nanoparticle-mediated Photothermal Therapy: Applications and Opportunities for Multimodal Cancer Treatment, Wiley Interdiscip. Rev. Nanomedicine Nanobiotechnology, Vol. 9, No. 4, 2017, pp. 1-16, https://doi.org/10.1002/wnan.1449.

[10] A. S. Kostyukov, A. E. Ershov, V. S. Gerasimov, S. A. Filimonov, I. L. Rasskazov, S. V. Karpov, Super-Efficient Laser Hyperthermia of Malignant Cells with Core-Shell Nanoparticles Based on Alternative Plasmonic Materials, J. Quant. Spectrosc. Radiat. Transf., Vol. 236, 2019, pp. 106599, https://doi.org/10.1016/j.jqsrt.2019.106599.

[11] G. Baffou, R. Quidant, C. Girard, Heat Generation In Plasmonic Nanostructures : Influence of Morphology, Vol. 94, No. 15, 2009, pp. 1-3, https://doi.org/10.1063/1.3116645.

[12] G. Baffou, R. Quidant, Thermo-plasmonics: Using Metallic Nanostructures as Nano-sources of Heat, Laser Photonics Rev., Vol. 7, No. 2, 2013, pp. 171-187, https://doi.org/10.1002/lpor.201200003.

[13] G. L. Liu, Y. Lu, J. Kim, J. C. Doll, L. P. Lee, Magnetic Nanocrescents as Controllable Surface-enhanced Raman Scattering Nanoprobes for Biomolecular Imaging, Adv. Mater., Vol. 17, No. 22, 2005, pp. 2683-2688, https://doi.org/10.1002/adma.200501064.

[14] C. Zheng et al., Theoretical Study on Narrow Fano Resonance of Nanocrescent for the Label-free Detection of Single Molecules and Single Nanoparticles, RSC Adv., Vol. 8, No. 7, 2018, pp. 3381-3391, https://doi.org/10.1039/c7ra12666b.

[15] D. Bang et al., Asymmetric Nanocrescent Antenna on Upconversion Nanocrystal, Nano Lett., Vol. 17, No. 11, 2017, pp. 6583-6590, https://doi.org/10.1021/acs.nanolett.7b02327.

[16] Z. Liao, B. Zhou, Y. Huang, S. Li, S. Wang, W. Wen, Fano Resonance Properties of Gold Nanocrescent Arrays, Appl. Opt., Vol. 53, No. 28, 2014, pp. 6431, https://doi.org/10.1364/AO.53.006431.

[17] Z. Li et al., The Fabrication of Long-range Ordered Nanocrescent Structures Based on Colloidal Lithography and Parallel Imprinting, Nanotechnology, Vol. 24, No. 10, 2013, pp. 1-9, https://doi.org/10.1088/0957-4484/24/10//105307.

[18] G. V. P. Kumar, Near-field Optical Resonance and Enhancement of A Plasmonic Nanocrescent Cylinder Tuned by A Proximal Plasmonic Nanostructure, J. Opt. Soc. Am. B, Vol. 29, No. 4, 2012, pp. 594, https://doi.org/10.1364/JOSAB.29.000594.

[19] X. H. Vu, M. Levy, T. Barroca, H. N. Tran, E. Fort, Gold Nanocrescents for Remotely Measuring and Controlling Local Temperature, Nanotechnology, Vol. 24, No. 32, 2013, https://doi.org/10.1088/0957-4484/24/32/325501.

[20] X. H. Vu et al., Measuring of Translational and Rotational Local Temperatures of A Single Gold Nanocrescent in Glycerol, Optik, Vol. 219, No. 12, 2019, pp. 165174, https://doi.org/10.1016/j.ijleo.2020.165174.

[21] M. F. Barroso et al., Gold Nanoparticles Covalently Assembled Onto Vesicle Structures as Possible Biosensing Platform, Beilstein J. Nanotechnol., Vol. 7, No. 5, 2016, pp. 655-663, https://doi.org/10.3762/bjnano.7.58.

[22] I. F. Sbalzarini, P. Koumoutsakos, Feature Point Tracking and Trajectory Analysis for Video Imaging in Cell Biology, J. Struct. Biol., Vol. 151, No. 2, 2005, pp. 182-195, https://doi.org/10.1016/j.jsb.2005.06.002.

[23] N. S. Cheng, Formula for the Viscosity of A Glycerol-water Mixture, Ind. Eng. Chem. Res., Vol. 47, No. 9, 2008, pp. 3285-3288, https://doi.org/10.1021/ie071349z.

[24] Y. Grasselli, G. Bossis, R. Morini, Translational and Rotational Temperatures of A 2D Vibrated Granular Gas in Microgravity, Eur. Phys. J. E, Vol. 38, No. 2, 2015, pp. 1-10, https://doi.org/10.1140/epje/i2015-15008-5.

[25] Y. Zhang, A. Barhoumi, J. B. Lassiter, N. J. Halas, Orientation-preserving Transfer and Directional Light Scattering from Individual Light-bending Nanoparticles, Nano Lett., Vol. 11, No. 4, 2011, pp. 1838-1844, https://doi.org/10.1021/nl2008357.

[26] N. A. Mirin, N. J. Halas, Light-Bending Nanoparticles, Nano Lett., Vol. 9, No. 3, 2009, pp. 1255-1259, https://doi.org/10.1021/nl900208z.

[27] H. Ueno et al., Simple Dark-field Microscopy with Nanometer Spatial Precision and Microsecond Temporal Resolution, Biophys. J., Vol. 98, No. 9, 2010, pp. 2014-2023, https://doi.org/10.1016/j.bpj.2010.01.011.

[28] J. Renn, Einstein's Invention of Brownian Motion, Ann. Der Phys., Vol. 517, No. S1, 2005, pp. 23-37, https://doi.org/10.1002/andp.200410131.

[29] J. Stepišnik, C. Mattea, S. Stap, A. Mohorič, Molecular Velocity Auto-correlations in Glycerol/Water Mixtures Studied by NMR MGSE Method, Vol. 553, No. 124171, 2020, pp. 1-12, https://doi.org/10.1016/j.physa.2020.124171.